Reaction Chemistry & Engineering

ROYAL SOCIETY OF CHEMISTRY

PAPER

View Article Online
View Journal | View Issue

Cite this: *React. Chem. Eng.*, 2021, **6**, 1819

Flow synthesis kinetics for lomustine, an anti-cancer active pharmaceutical ingredient

Samir Diab, † Mateen Raiyat and Dimitrios I. Gerogiorgis *

Received 7th May 2021,
Accepted 19th July 2021

DOI: 10.1039/d1re00184a

rsc.li/reaction-engineering

Continuous flow synthesis of active pharmaceutical ingredients (APIs) can offer access to process conditions that are otherwise hazardous when operated in batch mode, resulting in improved mixing and heat transfer, which enables higher yields and greater reaction selectivity. Reaction kinetic parameter estimation from flow synthesis data is an essential activity for the development of process models for drug substance manufacturing unit operations and systems, facilitating a reduction of experimental effort and accelerating development. The flow synthesis of lomustine, an anti-cancer API, in two flow reactors (carbamylation + nitrosation stages) was recently demonstrated by Jaman *et al.* (*Org. Process Res. Dev.*, 2019, **23**, 334). In this study, we postulate kinetic rate laws based on hereby proposed reaction mechanisms presented for the first time in the literature for this API synthesis. We then perform kinetic parameter regression for the proposed rate laws, on the basis of published data, towards establishing reactor models. For the carbamylation (irreversible reaction), we compare two candidate reaction rate laws, an overall third-order rate law (first-order in each reagent) deriving best fit. For the nitrosation, we propose two substitution reactions on the basis of published mechanisms (a rate-limiting equilibrium step, followed by a fast irreversible reaction) with very good model fit.

Introduction

Background

The number of people living with cancer and the number of cancer-related deaths have increased significantly over the last 30 years[1,2] (Fig. 1). Global spending on cancer treatment and prices of anti-cancer drugs have also rapidly increased.[3] Although there are many convoluted factors affecting drug prices,[4,5] efficient manufacturing can help to reduce the cost of production of medicines with societal and economic impact. Streamlining active pharmaceutical ingredient (API) manufacturing and accelerating process development can significantly reduce development costs towards this end.

Flow synthesis of active pharmaceutical ingredients

Flow synthesis demonstrations for a variety of APIs and their intermediates has received significant attention over the past decade. Development of flow technology and flow synthetic routes towards continuous manufacturing has rapidly increased due to the wide variety of chemical processes whose performance (productivity, quality, *etc.*) can be improved or intensified by switching from batch to continuous operation. There are several reviews documenting the rapid development of flow technology for fine chemical and pharmaceutical products.[6–12]

Table 1 summarises the various flow synthesis demonstrations of different anti-cancer APIs in the literature. However, deciding whether to operate in batch or continuous mode is non-trivial. For example, reactions with slow kinetics are better suited to batch operation and the existence of multiple phases can limit the benefits of operating in one mode *vs.* the other.[13,14] Moreover, if an existing process route has acceptable performance with respect to yield, scale, process time, purity *etc.*, and can be operated safely, then switching operating mode is not worthwhile. Judicious process selection and design is imperative for successful continuous process implementation.[15]

Reaction modelling to streamline process development

Mathematical modelling and be used to reduce experimental effort involved in process development and design. Despite the widespread adoption of modelling approaches in general, industrial pharmaceutical development is still dominated by experimental approaches; this is in part due to the fact that new projects are constantly being begun and terminated depending on the company's portfolio regarding prioritised assets, challenges in clinical and process development, *etc.*

Traditionally, the definition of the process optimum and the control strategy are supported by design of experiments (DoE) approaches which are used to construct empirical

Institute for Materials and Processes (IMP), School of Engineering, University of Edinburgh, The King's Buildings, Edinburgh, EH9 3FB, Scotland, UK.
E-mail: D.Gerogiorgis@ed.ac.uk
† Present affiliation: GlaxoSmithKline (GSK), Ware, SG12 0DP, UK.

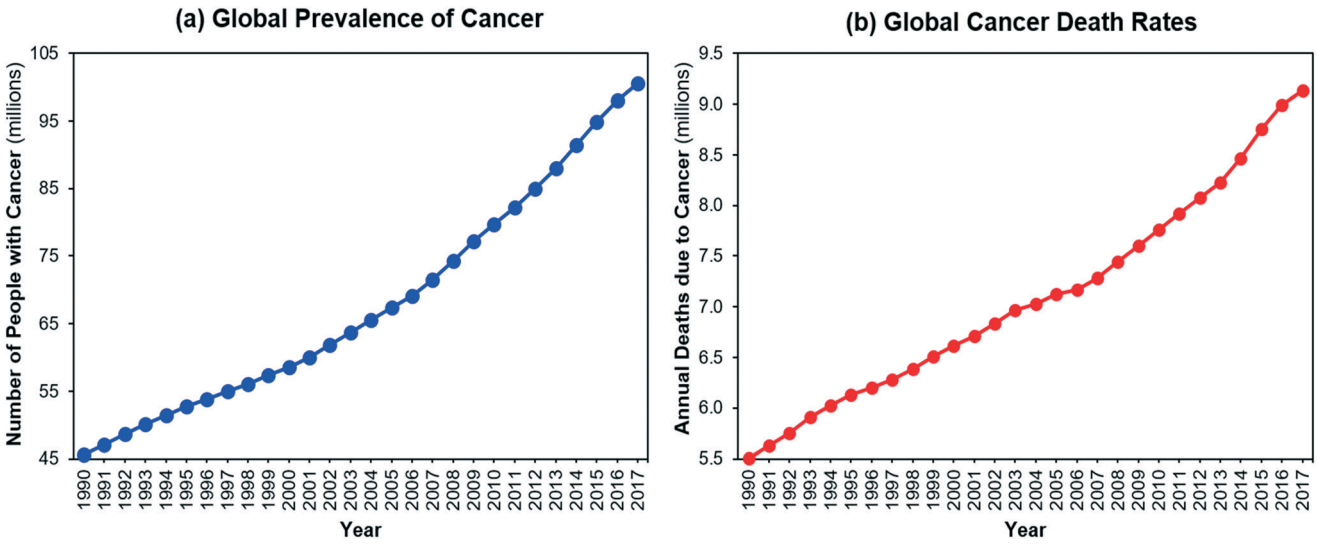

Fig. 1 (a) Global prevalence of cancer, (b) global death rates due to cancer.[2]

Table 1 Literature demonstrations of flow syntheses of APIs used in cancer treatment

#	API	Treatment	No. reactions	Intermediate separations?	Yield [%]	Capacity [g h^{-1}]	Ref.
1	Imatinib	Gastrointestinal stromal tumours	6	Y	69	[—]	16
2	Imatinib	Gastrointestinal stromal tumours	3	N	58	0.327	17
3	Tasisulam	Breast + ovarian cancer	3	N	90	5.200	18, 19
4	Tamoxifen	Breast cancer	5	N	84	8.287	20
5	Lomustine	Brain tumours Hodgkin's lymphoma	2	Y	63	0.110	21
6	Prexasertib	Acute myeloid leukaemia	3	Y	75–85	0.023	22
7	2-Fluoroadenine	Tumour prevention	1	N	82	120	23

models.[24] Despite their value and the advances in high throughput experimentation technologies,[25] they are not always the most suitable approaches to complex nonlinear problems typically encountered in pharmaceutical process systems. Moreover, they are generally resource-intensive.

Mechanistic and first-principles modelling approaches can provide deeper process understanding during development and design stages as well as definition of control strategies. The benefits of developing such models vary depending on the stage of development, but broadly include: (a) enhanced process understanding; (b) reducing experimental effort; (c) aiding process design; (d) sensitivity analysis; (e) design space elucidation; (f) process optimisation; (g) aiding scale-up.

Mechanistic modelling approaches are generally well-developed for reactor design and such models can be the basis of better-designed processes. In order to develop reactor models, it is fundamental to develop an understanding of: (a) reaction mechanisms and kinetics, including rate law parameters as well as interphase mass transfer, equilibria and mixing effects; (b) reaction thermodynamics; (c) dispersion effects and gradients; (d) mass and energy balances. Without these (either specific knowledge or valid assumptions therein), a detailed mechanistic understanding of a reaction remains elusive. Table 2 summarises different literature demonstrations of reaction kinetic parameter estimation for flow reaction model development, specifically for pharmaceutical small molecule synthesis.

This study

One example of an anti-cancer API with demonstrated continuous flow synthesis (Table 1) is lomustine, used for the treatment of brain tumours and Hodgkin's lymphoma.[21] Between 2013–2019, the cost of lomustine increased from 50 to 768 USD per capsule.[48] Herein, we use the available published reaction data for the lomustine flow synthesis[21] in order to postulate reaction mechanisms for each synthetic stage (informed by similar reactions in the literature) and perform kinetic parameter estimation towards reactor modelling for a drug substance manufacturing system model.

The remainder of this paper is structured as follows. First, we describe the published flow synthesis process of lomustine, including the equipment configuration and materials used.[21] We then postulate the reaction mechanisms of these steps as a basis for their proposed rate laws. The kinetic parameter estimation problem is then mathematically defined. The regressed kinetic parameters for the proposed rate laws are then presented with critical discussion of the methodology and results, followed by the conclusions of this study.

Table 2 Examples of reaction kinetic modelling for API flow syntheses in the literature

#	API	Application	Parameters regressed	Kinetic modelling benefits	Ref.
1	API	(—)	Isothermal rate constant, k_R	Reaction modelling + optimisation, process selection	26
2	API	(—)	Arrhenius pre-exponential factor, k_0 Activation energy, E_a	Reactor design + scaleup	27
3	Artemether	Antimalarial	Arrhenius pre-exponential factor, k_0 Activation energy, E_a Rate law	Reaction modelling + optimisation	28
4	Ibuprofen	Analgaesic	Isothermal rate constant, k_R Rate law	Continuous process simulation + optimisation	29, 30
5	Artemisinin	Antimalarial	Isothermal rate constant, k_R	Continuous process model simulation + optimisation	31, 32
6	Diphenhydramine	Antihistamine	Isothermal rate constant, k_R Rate law	Continuous process model simulation	33
7	Aziridines	Cancer therapy	Arrhenius pre-exponential factor, k_0 Activation energy, E_a	Reaction modelling + optimisation	34
8	Pyroles	Precursor	Arrhenius pre-exponential factor, k_0 Activation energy, E_a Rate law	Minimise number of experiments to characterise kinetic model	35
9	Int.	(—)	Arrhenius pre-exponential factor, k_0 Activation energy, E_a	Reaction modelling + optimisation	36
10	Abemaciclib	Anticoagulant	Arrhenius pre-exponential factor, k_0 Activation energy, E_a	Reaction modelling + optimisation	37
11	Rufinamide	Antiepileptic	Isothermal rate constant, k_R	Continuous process simulation	38
12	Thiazolidine Int.	Diabetes	Arrhenius pre-exponential factor, k_0 Activation energy, E_a	Reaction solvent selection	39
13	Glitazone	Diabetes	Arrhenius pre-exponential factor, k_0 Activation energy, E_a	Reaction solvent selection	40
14	Tryptophol	Sleep inducing	Arrhenius pre-exponential factor, k_0 Activation energy, E_a	Reaction modelling + optimisation	41
15	Atropine	Nerve agents + pre-surgical procedures	Isothermal rate constant, k_R Rate law	Continuous process simulation + optimisation	42, 43
16	Nevirapine	Anti-HIV	Arrhenius pre-exponential factor, k_0 Activation energy, E_a	Continuous process simulation + optimisation	44
17	Dolutegravir Int.	Anti-HIV	Arrhenius pre-exponential factor, k_0 Activation energy, E_a	Enable CFD modelling of flow reactor	45
18	Atropine	Nerve agents + pre-surgical procedures	Arrhenius pre-exponential factor, k_0 Activation energy, E_a	Model predictive control of continuous API manufacturing	46
19	API	(—)	Isothermal rate constant, k_R	Reaction modelling + optimisation	47

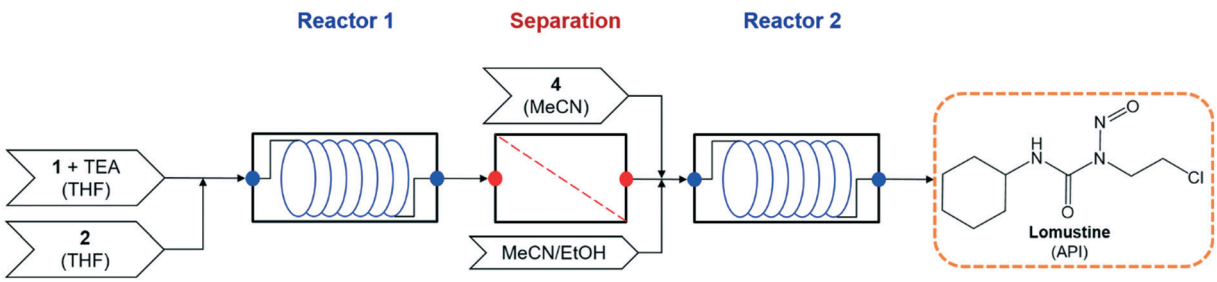

Fig. 2 Process flowsheet for flow synthesis of lomustine.[21]

Lomustine flow synthesis

The demonstrated continuous flow synthesis of lomustine (1-(2-chloroethyl)-3-cyclohexyl-1-nitrosourea) is performed in two flow reactors, with an intermediate purification to change reaction solvents[21] – the process flowsheet is shown in Fig. 2.

The overall reaction scheme is shown in Fig. 3. First, the carbamylation of cyclohexylamine (**1**, 0.5 mol L^{-1}, 1 equiv.) by 1-chloro-2-isocyanatoethane (**2**, 1.4 equiv.) in the presence of triethylamine (TEA, 1 equiv.) occurs in reactor 1 to form 1-(2-chloroethyl)-3-cyclohexylurea intermediate (**3**); reactor 1 is operated at T = 50 °C with tetrahydrofuran (THF) as the reaction solvent. Reaction data[21] is available at residence times, $\tau_1 = \{0, 10, 30, 60\}$ s.

In reactor 2, Int. **3** undergoes nitrosation with *tert*-butyl nitrite (**4**) to form lomustine (API); Int. **3** (1 equiv., 1 mol L^{-1}) in a mixture of 3.72 : 1 [v/v] acetonitrile/ethanol (MeCN/EtOH) solvent mixture reacts with **4** (3 equiv. in MeCN) at T = 50 °C

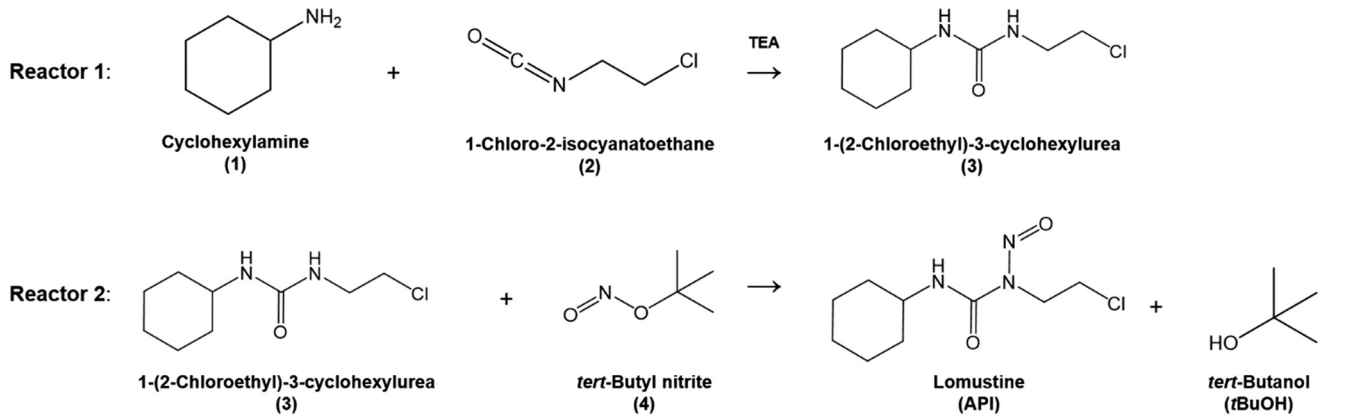

Fig. 3 Flow reaction scheme for continuous synthesis of lomustine (API).[21]

Table 3 Material properties of components used in lomustine flow synthesis (N.A. = not available)

Species	Role	CAS #	Formula	MW [g mol^{-1}]	Density [g mL^{-1}]	Melting point [°C]	Boiling point [°C]
1	Reagent	108-91-8	$C_6H_{13}N$	99.17	0.865	−17.7	134.0
2	Reagent	1943-83-5	$C_5H_6ClNO_3$	163.56	1.237	N.A.	135.0
TEA	Reagent/base	121-44-8	$C_6H_{15}N$	101.19	0.726	−114.7	89.3
3	Intermediate	13908-11-7	$C_9H_{17}ClN_2O$	204.70	1.110	N.A.	N.A.
THF	Solvent	109-99-9	C_4H_8O	72.11	0.889	−108.4	66.0
4	Reagent	463-04-7	$C_4H_9NO_2$	103.12	0.867	N.A.	62.0
API	Product	13010-47-4	$C_9H_{16}ClN_3O_2$	233.70	1.400	90.0	N.A.
MeCN	Solvent	75-05-08	C_2H_3N	41.05	0.786	−45.0	82.0
EtOH	Solvent	64-17-5	C_2H_6O	46.07	0.789	−114.1	78.4

to form API and *tert*-butanol (*t*BuOH) by-product. Reaction data is available at residence times, $\tau_2 = \{0, 30, 60, 180, 300, 480\}$ s in the literature demonstration.[21] Full details and properties of these key feed materials, intermediates and products involved in the flow synthesis of lomustine are summarised in Table 3.

Reaction mechanisms and kinetic model equations

Reaction rate and material balances

The following assumptions are made in the reaction kinetic modelling presented in this study:

(a) Only the considered reactions occur in their corresponding reactors, *i.e.*, carbamylation in reactor 1, nitrosation in reactor 2, in the liquid phase only;[21]

(b) All reactions are isothermal (both reactors operated at $T = 50$ °C) as per the demonstrated flow synthesis;[21]

(c) Ideal mixing is achieved in each reactor, *i.e.*, radial concentration gradients are negligible, as well as axial dispersion and temperature gradients (an appropriate assumption given the scale of the considered experimental flow synthesis demonstration);[21]

(d) Constant volumetric flowrates in all reactors, *i.e.*, consumption/formation of species due to chemical reaction does not alter the mixture volume;

(e) Isothermal reactor operation is considered, and the requisite heat transfer is assumed perfectly efficient, ensured by appropriate heat transfer media provision and flow (no heat accumulation);

(f) Reactor operating temperatures are kept safely below solvent boiling points – this has indeed been confirmed as per the comparison thereof *vs.* solvent thermophysical properties (Table 3);

(g) Precipitation of reagents, intermediates and products does not occur, on account of the fact that such phenomena are not reported in the experimental demonstration, rendering this assumption valid.[21]

The proposed rate laws and regressed kinetic parameters should apply to both batch and flow modes of operation given these assumptions. Upon scale up, care should be taken to ensure that the intrinsic kinetics still hold; they could potentially vary due to other reaction rate-limiting barriers such as heat transfer and gradients within the reactor.

Under the listed assumptions, the general reaction rate equation is given by eqn (1). Here, r_R = rate of reaction R, k_R = isothermal rate constant of reaction R (at $T = 50$ °C for both reactors[21]), N_C = total number of species, $C_i(\tau)$ = concentration of species i at residence time τ_l in reactor l for a total $N_{reactor}$ reactors, $\alpha_{i,R}$ = order of species i in reaction R, N_{rxn} = total number of reactions, $\boldsymbol{C}$ = vector of species concentrations. The overall order of reaction, $\alpha_{T,R}$ is the sum of the individual species' orders, $\alpha_{i,R}$, (eqn (2)).

$$r_R(\tau_l, \boldsymbol{C}) = k_R \prod_{i=1}^{N_C} C_i(\tau_l)^{\alpha_{i,R}} \quad \begin{matrix} \forall l \in N_{reactor} \\ \forall R \in N_{rxn} \end{matrix} \tag{1}$$

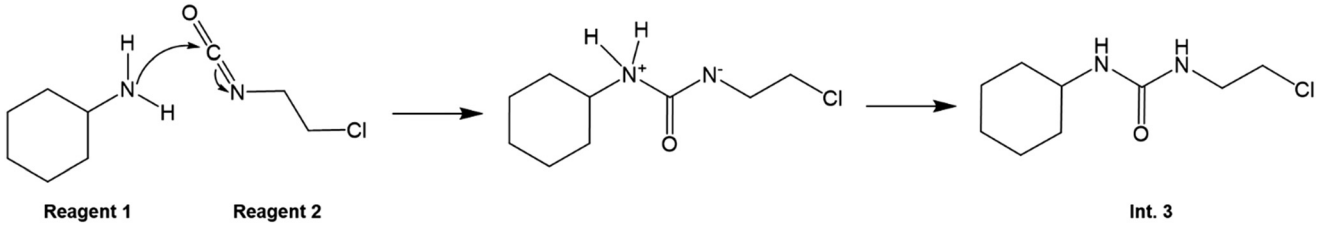

Fig. 4 Carbamylation (reaction 1) mechanism to form Int. **3**.

$$\alpha_{T,R} = \sum_{i=1}^{N_C} \alpha_{i,R} \quad \forall R \in N_{rxn} \tag{2}$$

The material balance of an ideally mixed tubular reactor with constant volumetric flowrate is described by a system of ordinary differential equations (ODEs), as per eqn (3). Here, $\nu_{i,R}$ = stoichiometric coefficient of species i in reaction R.

$$\frac{dC_i(\tau_l)}{d\tau_l} = \sum_{R=1}^{N_{rxn}} \nu_{i,R} r_R(\tau_l, \boldsymbol{C}) \quad \begin{matrix} \forall i \in N_C \\ \forall l \in N_{reactor} \end{matrix} \tag{3}$$

These equations are now expanded in the context of the proposed rate laws for reactions for the considered lomustine flow synthesis.[21]

Reactor 1: carbamylation

The mechanism of reaction 1 is illustrated in Fig. 4. The carbamylation (reaction 1) in reactor 1 involves the interaction between a nucleophile (the lone electron pair on the nitrogen atom on **1**) and an electrophile (the O═C═N carbon centre on **2**). This then leads to a tetrahedral intermediate, in which proton transfer then occurs from one nitrogen atom (which has a positive charge due to the extra proton) to the other one (which has a free electron from the opening of the C═N bond on **1**), resulting in Int. **3**.

There is also the possibility that the lone electron pair on the nitrogen atom of **1** can attack the carbon centre adjacent to the chlorine atom on **2**. This would result in HCl formation, which would impede the desired reaction of **1** with **2** to form Int. **3**. The role of TEA in the reaction is not explained in the published lomustine flow synthesis,[21] but it is possible that the goal is the prevention of the said effect.

Table 4 Stoichiometric coefficients (ν) and reaction orders (α) for different species in rate equations

Reactor	Reaction		Species, i								
l	R		**1**	**2**	TEA	**3**	**4**	**4a**	**4b**	API	tBuOH
1	1 (Opt. a)	$\nu_{i,1}$	−1	−1	−1	+1	0	0	0	0	0
		$\alpha_{i,1}$	+1	+1	0	0	0	0	0	0	0
	1 (Opt. b)	$\nu_{i,1}$	−1	−1	−1	+1	0	0	0	0	0
		$\alpha_{i,1}$	+1	+1	+1	0	0	0	0	0	0
2	2f	$\nu_{i,2f}$	0	0	0	0	−1	+1	+1	0	0
		$\alpha_{i,2f}$	0	0	0	0	+1	0	0	0	0
	2r	$\nu_{i,2r}$	0	0	0	0	+1	−1	−1	0	0
		$\alpha_{i,2r}$	0	0	0	0	0	+1	+1	0	0
	3	$\nu_{i,3}$	0	0	0	−1	0	0	−1	+1	+1
		$\alpha_{i,3}$	0	0	0	+1	0	0	+1	0	0

Carbamylations are fast and irreversible.[49,50] We compare two candidate rate laws: (a) first-order in each of **1** and **2** (*i.e.*, overall second-order, $\alpha_{T,R}$ = 2) and (b) first-order in each of **1**, **2** and TEA (*i.e.*, overall third-order, $\alpha_{T,R}$ = 3). Candidate rate law (b) is considered as TEA is in 1 : 1 molar equivalent with reagent **1**, which is key in facilitating the carbamylation and thus the rate law may be dependent on its concentration[51] in addition to the key reagents **1** and **2**.

$$\text{Option (a): } r_1(\tau_1, \boldsymbol{C}) = k_1 C_1(\tau_1) C_2(\tau_1) \tag{4}$$

$$\text{Option (b): } r_1(\tau_1, \boldsymbol{C}) = k_1 C_1(\tau_1) C_2(\tau_1) C_{TEA}(\tau_1) \tag{5}$$

Expanding eqn (2), the material balances in reactor 1 are thus described by eqn (6)–(8). Stoichiometric coefficients and reaction orders for each species are listed in Table 4.

$$\frac{dC_1(\tau_1)}{d\tau_1} = -r_1(\tau_1, \boldsymbol{C}) \tag{6}$$

$$\frac{dC_2(\tau_1)}{d\tau_1} = -r_1(\tau_1, \boldsymbol{C}) \tag{7}$$

$$\frac{dC_3(\tau_1)}{d\tau_1} = +r_1(\tau_1, \boldsymbol{C}) \tag{8}$$

Reactor 2: nitrosation

The overall synthesis of API in reactor 2 is the nitrosation involving **3** and **4** in aqueous solution. Detailed kinetic rate law equations of such nitrosation reactions for the considered system are not published in the literature to the best of the authors' knowledge. Here, we propose a reaction mechanism based on other studies for similar nitrosations and postulate the rate law equations, for which kinetic parameters are regressed using the available published experimental data for lomustine synthesis.[21]

The considered reaction mechanism for the nitrosation of Int. **3** by **4** involves radical disproportionation of **4** to tBuO$^\bullet$ (Int. **4a**) and $^\bullet$N═O (Int. **4b**), which has been reported to occur in aqueous conditions.[52,53] Thereafter, Int. **4a** interacts with a N–H bond on Int. **3**, as illustrated in Fig. 5, forming tBuOH as well as another radical, which subsequently reacts with Int. **4b**, in order to form the API (lomustine).

The reaction scheme (Fig. 5) shows the tBuO$^\bullet$ radical interacting with the N–H bond on the chlorine side of the C═O bond on the Int. **3** molecule as opposed to that adjacent to the

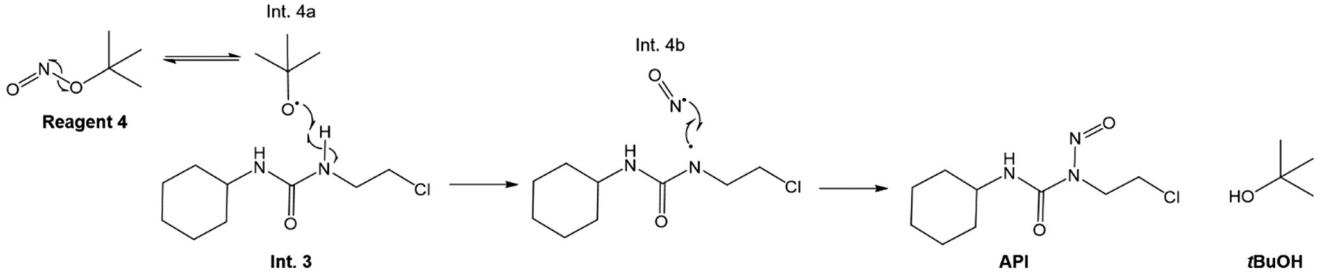

Fig. 5 Overall nitrosation reaction mechanism in reactor 2 to form API.[52]

cyclohexyl group. It is possible that the N–H bond adjacent to the cyclohexyl ring is being stabilised by the said group, leading to the *t*BuO$^{\bullet}$ radical preferentially interacting with the N–H bond on the chlorine side of the C═O bond. The authors suggest that the proposed reaction mechanisms be corroborated with additional data confirming these hypotheses.

The radical formation is considered an equilibrium reaction with forward and backward reaction rates, r_{2f} and r_{2r}, respectively, with rate constants, k_{2f} and $k_{2r} = k_{2f}/K_{eq}$, respectively, where K_{eq} therein has been defined as the radical disproportionation equilibrium constant. Reaction 3 is therefore considered an overall irreversible (forward only) reaction involving Int. **3**, Int. **4a** and Int. **4b**, which proceeds to form the API (lomustine) as well as *t*BuOH (a by-product), as illustrated in the final stage of Fig. 5. The proposed kinetic rate laws for the foregoing reactions are therefore now described by eqn (9)–(11).

$$r_{2f}(\tau_2, \boldsymbol{C}) = k_{2f} C_4(\tau_2) \tag{9}$$

$$r_{2r}(\tau_2, \boldsymbol{C}) = \frac{k_{2f}}{K_{eq}} C_{4a}(\tau_2) C_{4b}(\tau_2) \tag{10}$$

$$r_3(\tau_2, \boldsymbol{C}) = k_3 C_3(\tau_2) C_{4b}(\tau_2) \tag{11}$$

Expanding from eqn (2), the resulting material balances in reactor 2 are as per eqn (12)–(14). Stoichiometric coefficients and reaction orders for reactor 2 are listed in Table 4.

$$\frac{dC_3(\tau_2)}{d\tau_2} = -r_3(\tau_2, \boldsymbol{C}) \tag{12}$$

$$\frac{dC_4(\tau_2)}{d\tau_2} = -r_{2f}(\tau_2, \boldsymbol{C}) + r_{2r}(\tau_2, \boldsymbol{C}) \tag{13}$$

$$\frac{dC_{API}(\tau_2)}{d\tau_2} = +r_3(\tau_2, \boldsymbol{C}) \tag{14}$$

With the proposed reaction mechanisms, we now formulate a parameter estimation problem for reaction kinetic parameter estimation.

Parameter estimation

The regression of reaction kinetic parameters from experimental data is a parameter estimation problem described as the minimisation of the sum of square errors in eqn (15). Here, f = objective function, N_{expt} = number of reaction experiments considered, N_C = number of species for which data is measured and being predicted by the kinetic model, N_P = number of time points at which experimental data is available, $C_{p,i,j}^{model}$ = model prediction of concentration of species i and time p in experiment j, $C_{p,i,j}^{expt}$ is the corresponding experimental value, $\tau_{p,j}$ = time p in experiment j, $\boldsymbol{\theta}$ = model parameter vector.

$$\min_{\boldsymbol{\theta}} f = \sum_{j=1}^{N_{expt}} \sum_{i=1}^{N_C} \sum_{p=1}^{N_P} \left[\frac{C_{p,i,j}^{model}(\tau_{p,j}, \boldsymbol{\theta}) - C_{p,i,j}^{expt}(\tau_{p,j})}{C_{p,i,j}^{expt}(\tau_{p,j})} \right]^2 \tag{15}$$

For each reaction, N_{expt} = 1. In reactor 1, N_C = 3 (species i = reagent **1**, reagent **2**, Int. **3**), N_P = 4; in reactor 2, N_C = 3 (species i = **3**, reagent **4**, API), N_P = 6. For reaction 1 occurring in reactor 1, the parameter vector in eqn (15) is $\boldsymbol{\theta} = k_1$. For Reactions 2 + 3 in reactor 2, the parameter vector in eqn (15) is $\boldsymbol{\theta} = [k_{2f}, K_{eq}, k_3]$.

The model equations and parameter estimation problem are coded in MATLAB. The system of ODEs is solved using *ode15s* (stiff ODE solver[54]) and the parameter estimation problem is solved using *lsqnonlin* (Levenberg–Marquardt algorithm,[55,56] default tolerance = 10^{-6}). Reactor 1 is simulated for a total τ = 60 s and reactor 2 is simulated for a total τ = 480 s, chosen as the maximum time at which reaction data is available in the experimental demonstrations.[21] All modelling is performed on an Intel® Core™ i-78665 CPU @ 1.90 GHz processor with 16.0 GB of RAM. In all cases, a single simulation took <1 s and the parameter estimation problem was solved in <10 s.

Results and discussion

Carbamylation (reaction 1)

The model fits for both candidate rate laws (options a and b) for reaction 1 in reactor 1 are shown in Fig. 6; parameter fits are summarised in Table 5 along with fitting confidence interval (CIs) and the corresponding coefficients of determination (R^2) for each concentration profile. It can be seen a better fit is obtained for option (b), however option (a) still provides good fit, albeit with lower confidence.

The yield of Int. **3** in reaction 1 is calculated as the ratio of molar concentration of Int. **3** at the end of the reaction *vs.* the initial molar concentration of limiting reagent (= Reagent **1**). The assumed rate law thus also results in different yields

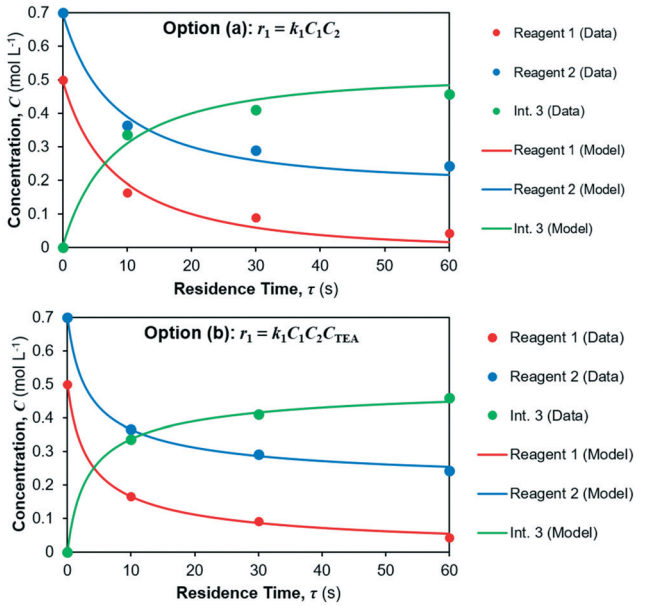

Fig. 6 Kinetic parameter fit for reaction 1. (a) Overall second-order rate law, (b) overall third-order rate law.

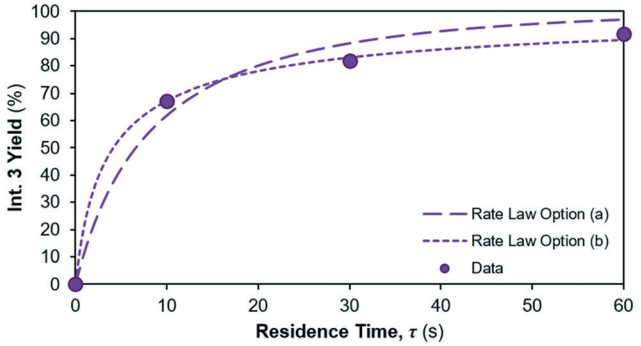

Fig. 7 Int. 3 yield profile for different reaction 1 rate law assumptions.

of Int. **3** *vs.* residence time, shown in Fig. 7; option (a) overpredicts the Int. **3** concentration (see model *vs.* data in Fig. 6a) compared to option (b), which fits better. Corroboration with additional data is required to confidently distinguish between the options.

Nitrosation (reactions 2 + 3)

The model fit for the considered reaction mechanism/rate laws for the reactions occurring in reactor 2 are shown in Fig. 8. Parameter fits are summarised in Table 6. The quality of fit is very high for the considered rate laws, however confidence in the parameter fits (= CI) is lower than for reaction 1. The yield of API from reactions 2 + 3 is calculated as the ratio of product (= API) obtained at the end of the reaction *vs.* the initial concentration of limiting reagent (= Int. **3**). The corresponding API yield profile is shown in Fig. 9.

As per our hypothesis, the equilibrium constant of reaction 2 is low, *i.e.*, the equilibrium is far to the left and thus reaction 2 is rate limiting with respect to API formation. Reaction 3 then proceeds very fast, as shown by the high value of rate constant k_3. This observed behaviour of a rate-limiting equilibrium step followed by a fast reaction is often observed in organic syntheses,[57,58] including nitrosation, as is occurring in reactions 2 + 3.[59,60]

Discussion

The proposed reaction mechanisms and rate laws fit the available data for each reaction very well; corroboration of the proposed rate laws can be accomplished by means of additional experimental effort towards data acquisition, which should ideally address: (a) spectroscopic identification of relevant intermediates for proposed reaction mechanisms, (b) high-resolution dynamic concentration measurements (especially at the onset of reactions, during which concentration gradients are steepest), (c) parametric (*e.g.* feed flowrates, reactor temperatures) variation. Obtaining such augmented datasets is beyond the scope of our kinetic analysis study; nevertheless, such an effort can certainly enhance our understanding of the reaction mechanisms for this particular API synthetic route.

A kinetic model is most often based on an assumed reaction mechanism whose rate equations are then to be validated *via* experimental data, possibly *via* similar reaction literature

Table 5 Regressed kinetic parameter values and model fit quality for carbamylation (reaction 1)

				Coefficient of determination (R^2)		
Parameter θ	Value	95% CI	Units	**1**	**2**	**3**
k_1 (Opt. a)	0.1906	±16.96%	[L mol^{-1} s^{-1}]	0.9820	0.9820	0.9820
k_1 (Opt. b)	0.9024	±6.75%	[L^2 mol^{-2} s^{-1}]	0.9988	0.9988	0.9988

Table 6 Regressed kinetic parameter values and model fit quality for nitrosation reaction (reactions 2 + 3)

					Coefficient of determination (R^2)		
Reaction	Parameter θ	Value	95% CI	Units	**3**	**4**	API
2	k_{2f}	0.5074	±19.00%	[s^{-1}]	0.9558	0.9715	0.9709
	K_{eq}	1.1798×10^{-5}	±16.70%	[mol L^{-1}]			
3	k_3	100.1360	±16.50%	[L mol^{-1} s^{-1}]			

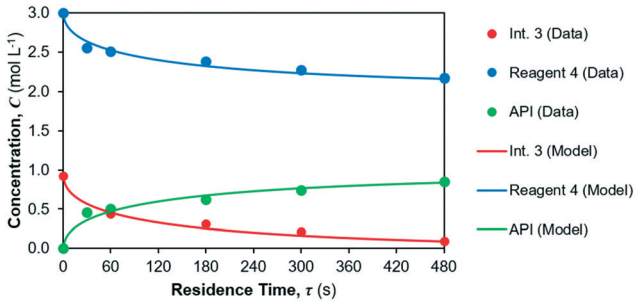

Fig. 8 Kinetic parameter fit for reactions 2 and 3 in reactor 2.

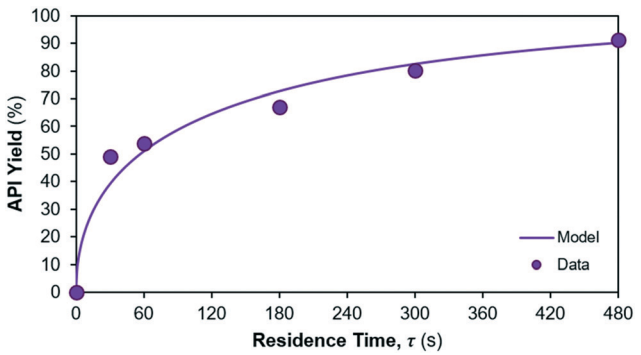

Fig. 9 API yield profile in reactor 2.

precedents. This validation does not ensure uniqueness or proof of the postulate, but has predictive value. The quality of fit for model parameters (best assessed by confidence intervals) strongly depends on data quality and quantity, and can indicate whether the assumed mechanism (thus: model structure) is correct, or if an alternative pathway may actually be occurring (assuming the parameter estimation algorithm and solver settings are suitably chosen to safeguard against local minimisation entrapment possibility).

Computational chemistry complements experiments in order to elucidate complex reaction phenomena. Density functional theory (DFT) is an established and efficient methodology[61] for studying and analysing mechanisms related to stereoselectivity,[62] organocatalysis,[63] and provides valuable assistance to spectroscopic[64] and other relevant investigations. A DFT approach may provide additional insight, but is beyond the scope of our present study. Various hurdles still remain to allow for its wider applicability and use, including the issue of successful predictions of transition structure geometry[65] (which are key to the reaction mechanisms proposed in this study), the selection of appropriate functionals[66] and the hazard of errors in kinetic parameter estimations[67] (also important in this study). It would be an exciting prospect for this kinetic parameter estimation study to motivate DFT analyses.

Conclusions

The demonstrated flow synthesis of lomustine and available reaction data were used to postulate candidate rate laws based on proposed reaction mechanisms for each synthesis step. For the carbamylation (irreversible reaction), we compare two candidate reaction rate laws, with an overall third-order rate law (first-order in each reagent) showing the best fit. For the nitrosation (in the first reactor), we propose two substitution reactions (one rate-limiting equilibrium step, one fast irreversible step) with very good model fit *vs.* published experimental data. Corroboration of the proposed mechanisms with computational chemistry (*e.g.* DFT) methods and/or additional experimentation can enhance understanding of the reaction mechanisms for this API synthetic route. The presented kinetic model can accelerate continuous reactor design, scale-up and optimisation of lomustine production.

Nomenclature

Acronyms

API	Active pharmaceutical ingredient
CI	Confidence interval
DFT	Density functional theory
DoE	Design of experiments
ODE	Ordinary differential equation

Chemical compounds

1	Cyclohexylamine
2	1-Chloro-2-isocyanatoethane
3	1-(2-Chloroethyl)-3-cyclohexylurea
4	*tert*-Butyl nitrite
4a	*t*BuO$^{\bullet}$ radical
4b	$^{\bullet}$N═O radical
EtOH	Ethanol
Int.	Intermediate
MeCN	Acetonitrile
*t*BuOH	*tert*-Butanol
TEA	Triethylamine
THF	Tetrahydrofuran

Symbols

Latin letters.

C	Concentration [mol L^{-1}]
$\boldsymbol{C}$	Vector of species concentrations [mol^{-1}]
E_a	Activation energy [J mol^{-1}]
f	Parameter estimation objective function [–]
K_{eq}	Equilibrium constant [mol L^{-1}]
k_0	Pre-exponential factor [L$^{\alpha T-1}$ mol$^{\alpha T-1}$ s^{-1}]
k_R	Isothermal rate constant of reaction R [L$^{\alpha T-1}$ mol$^{\alpha T-1}$ s^{-1}]
MW	Molecular weight [g mol^{-1}]
N_C	Number of components [–]
N_{expt}	Number of experiments [–]
N_P	Number of data points [–]
$N_{reactor}$	Number of reactors [–]
N_{rxn}	Number of reactions [–]
R^2	Coefficient of determination [–]
r_R	Rate of reaction R [mol L^{-1} s^{-1}]

T Temperature [°C]
$\nu_{i,R}$ Stoichiometric coefficient of species i in reaction R [–]

Greek letters.
$\alpha_{i,R}$ Reaction order of species i in reaction R [–]
$\alpha_{T,R}$ Overall order of reaction R [–]
τ Residence time [s]
$\boldsymbol{\theta}$ Parameter vector

Author contributions

Samir Diab: methodology, software, formal analysis, investigation, writing – original draft + review & editing, visualisation. Mateen Raiyat: methodology, software, formal analysis, investigation, writing – original draft, visualisation. Dimitrios I. Gerogiorgis: conceptualisation, methodology, writing – review & editing, visualisation, supervision, project administration, funding acquisition.

Conflicts of interest

There are no conflicts of interest to declare.

Acknowledgements

The authors gratefully acknowledge the Engineering and Physical Sciences Research Council (EPSRC) *via* a Doctoral Training Partnership PhD Fellowship (Grant #EP/N509644/1) to S. D., the support of the Great Britain Sasakawa and Nagai Foundations and a Royal Society (RS) Short Industrial Fellowship (2020–2021) to D. I. G (SIF\R1\201041). Tabulated and cited literature data suffice for reproduction of all original process simulation and parameter estimation results; no other supporting data are required for reproducibility.

References

1 A. Jemal, E. M. Ward, C. J. Johnson, K. A. Cronin, J. Ma, A. B. Ryerson, A. Mariotto, A. J. Lake, R. Wilson, R. L. Sherman, R. N. Anderson, S. J. Henley, B. A. Kohler, L. Penberthy, E. J. Feuer and H. K. Weir, *JNCI, J. Natl. Cancer Inst.*, 2017, **109**, djx030.
2 M. Roser and H. Ritchie, "Cancer", https://ourworldindata.org/cancer, (Accessed: 18th March 2021).
3 P. B. Bach, *N. Engl. J. Med.*, 2009, **360**, 626.
4 N. P. Tallapragada, *J. Law Biosci.*, 2016, **3**, 238.
5 J. A. DiMasi, H. G. Grabowski and R. W. Hansen, *J. Health Econ.*, 2016, **47**, 20.
6 M. Baumann and I. R. Baxendale, *Beilstein J. Org. Chem.*, 2015, **11**, 1194.
7 M. B. Plutschack, B. Pieber, K. Gilmore and P. H. Seeberger, *Chem. Rev.*, 2017, **117**, 11796.
8 J. Britton and C. L. Raston, *Chem. Soc. Rev.*, 2017, **52**, 10159.
9 R. O. M. A. de Souza and P. Watts, *J. Flow Chem.*, 2017, **7**, 146.
10 L. Malet-Sanz and F. Susanne, *J. Med. Chem.*, 2012, **55**, 4062.
11 I. R. Rossetti and M. Compagnoni, *Chem. Eng. J.*, 2016, **296**, 56.
12 V. R. L. J. Bloemendal, M. A. C. H. Janssen, J. C. M. van Hest and F. P. J. T. Rutjes, *React. Chem. Eng.*, 2020, **5**, 1186.
13 J. G. Costandy, T. F. Edgar and M. Baldea, *Ind. Eng. Chem. Res.*, 2019, **58**, 13718.
14 P. Bana, R. Örkényi, K. Lövei, Á. Lakó, G. I. Túrós, J. Éles, F. Faigl and F. I. Greiner, *Bioorg. Med. Chem.*, 2017, **25**, 6180.
15 S. Diab and D. I. Gerogiorgis, *Pharmaceutics*, 2020, **12**, 235.
16 M. D. Hopkin, I. R. Baxendale and S. V. Ley, *Chem. Commun.*, 2010, **46**, 2450.
17 W. C. Fu and T. F. Jamison, *Org. Lett.*, 2019, **21**, 6112.
18 T. D. White, K. D. Berglund, J. M. Groh, M. D. Johnson, R. D. Miller and M. H. Yates, *Org. Process Res. Dev.*, 2012, **16**, 939.
19 C. S. Polster, K. P. Cole, C. L. Burcham, B. M. Campbell, A. L. Frederick, M. M. Hansen, M. Harding, M. R. Heller, M. T. Miller, J. L. Phillips, P. M. Pollock and N. Zaborenko, *Org. Process Res. Dev.*, 2014, **18**, 1295.
20 P. R. D. Murray, D. L. Browne, J. C. Pastre, C. Butters, D. Guthrie and S. V. Ley, *Org. Process Res. Dev.*, 2013, **17**, 1192.
21 Z. Jaman, T. J. P. Sobreira, A. Mufti, C. R. Ferreira, R. G. Cooks and D. H. Thompson, *Org. Process Res. Dev.*, 2019, **23**, 334.
22 K. P. Cole, J. M. C. Groh, M. D. Johnson, C. L. Burcham, B. M. Campbell, W. D. Diseroad, M. R. Heller, J. R. Howell, N. J. Kallman, T. M. Koenig, S. A. May, R. D. Miller, D. Mitchell, D. P. Myers, S. S. Myers, J. L. Phillips, C. S. Polster, T. D. White, J. Cashman, D. Hurley, R. Moylan, P. Sheehan, R. D. Spencer, K. Desmond, P. Desmond and O. Gowran, *Science*, 2017, **356**, 1144.
23 N. Salehi Marzijarani, D. R. Snead, J. P. McMullen, F. Lévesque, M. Weisel, R. J. Varsolona, Y. Lam, Z. Liu and J. R. Naber, *Org. Process Res. Dev.*, 2019, **23**, 1522.
24 N. S. Politis, P. Colombo, G. M. Colombo and D. Rekkas, *Drug Dev. Ind. Pharm.*, 2017, **43**, 889–901.
25 S. M. Mennen, C. Alhambra, C. L. Allen, M. Barberis, S. Berritt, T. A. Brandt, A. D. Campbell, J. Castañón, A. H. Cherney, M. Christensen, D. B. Damon, J. Eugenio de Diego, S. García-Cerrada, P. García-Losada, R. Haro, J. Janey, D. C. Leitch, L. Li, F. Liu, P. C. Lobben, D. W. C. MacMillan, J. Magano, E. McInturff, S. Monfette, R. J. Post, D. Schultz, B. J. Sitter, J. M. Stevens, I. I. Strambeanu, J. Twilton, K. Wang and M. A. Zajac, *Org. Process Res. Dev.*, 2019, **23**, 1213–1242.
26 A. E. Rubin, S. Tummala, D. A. Both, C. Wang and E. J. Delaney, *Chem. Rev.*, 2006, **106**, 2794.
27 N. Kockmann and D. Roberge, *Chem. Eng. Process*, 2011, **50**, 1017.
28 P. Yaseneva, D. Plaza, X. Fan, K. Loponov and A. Lapkin, *Catal. Today*, 2015, **239**, 90.
29 H. G. Jolliffe and D. I. Gerogiorgis, *Chem. Eng. Res. Des.*, 2015, **97**, 175.
30 H. G. Jolliffe and D. I. Gerogiorgis, *Ind. Eng. Chem. Res.*, 2017, **56**, 4357.
31 H. G. Jolliffe and D. I. Gerogiorgis, *Chem. Eng. Res. Des.*, 2016, **112**, 310.
32 H. G. Jolliffe and D. I. Gerogiorgis, *Comput. Chem. Eng.*, 2017, **103**, 218.

33 S. Diab and D. I. Gerogiorgis, *Org. Process Res. Dev.*, 2017, **21**, 924.
34 A. Echtermeyer, Y. Amar, J. Zakrzewski and A. Lapkin, *Beilstein J. Org. Chem.*, 2017, **13**, 150.
35 K. C. Aroh and K. F. Jensen, *React. Chem. Eng.*, 2018, **3**, 94–101.
36 H. Keles, F. Susanne, H. Livingstone, S. Hunter, C. Wade, R. Bourdon and A. Rutter, *Org. Process Res. Dev.*, 2017, **21**, 1761.
37 M. O. Frederick, M. A. Pietz, D. P. Kjell, R. N. Richey, G. A. Tharp, T. Touge, N. Yokoyama, M. Kida and T. Matsuo, *Org. Process Res. Dev.*, 2017, **21**, 1447.
38 S. Diab and D. I. Gerogiorgis, *Comput. Chem. Eng.*, 2018, **111**, 102.
39 R. R. de Oliveira Silva, P. V. C. Calvo, M. Fernandes da Silva, C. Solisio, A. Converti and M. S. Alves Palma, *Chem. Eng. Technol.*, 2019, **42**, 465.
40 D. da Pinheiro, R. R. Silva, R. R. de Oliveira, P. V. C. Calvo, M. Fernandes da Silva, A. Converti and M. S. A. Palma, *Chem. Eng. Technol.*, 2018, **41**, 1800.
41 Y. R. Dubhashe, V. M. Sawant and V. G. Gaikar, *Ind. Eng. Chem. Res.*, 2018, **57**, 2787.
42 S. Diab, N. Mytis, A. G. Boudouvis and D. I. Gerogiorgis, *Comput. Chem. Eng.*, 2019, **124**, 28.
43 S. Diab and D. I. Gerogiorgis, *AIChE J.*, 2019, **65**, e16738.
44 S. Diab, D. T. McQuade, B. F. Gupton and D. I. Gerogiorgis, *Org. Process Res. Dev.*, 2019, **23**, 320.
45 C. T. Armstrong, C. Q. Pritchard, D. W. Cook, M. Ibrahim, B. K. Desai, P. J. Whitham, B. J. Marquardt, Y. Chen, J. T. Zoueu, M. J. Bortner and T. D. Roper, *React. Chem. Eng.*, 2019, **4**, 634.
46 A. Nikolakopoulou, M. von Andrian and R. D. Braatz, *2020 American Control Conference*, 2020, p. 2778.
47 C. J. Taylor, M. Booth, J. A. Manson, M. J. Willis, G. Clemens, B. A. Taylor, T. W. Chamberlain and R. A. Bourne, *Chem. Eng. J.*, 2020, 127017.
48 J. W. Taylor, T. Armstrong, A. H. Kim, M. Venere, A. Acquaye, D. Schrag and P. Y. Wen, *Neuro. Oncol.*, 2019, **21**, 1.
49 G. R. Stark, *J. Biol. Chem.*, 1964, **239**, 1411.
50 D. G. Smyth, *J. Biol. Chem.*, 1967, **242**, 1579.
51 J. Burés, *Top. Catal.*, 2017, **60**, 631.
52 A. Dahiya, A. K. Sahoo, T. Alam and B. K. Patel, *Chem. – Asian J.*, 2019, **14**, 4454.
53 S. A. Glover, A. Goosen, C. W. McCleland, F. R. Vogel and S. African, *J. Chem.*, 1981, **34**, 96.
54 L. F. Shampine, *Numerical Solution of Ordinary Differential Equations*, CRC Press, Boca Raton, 1st edn, 1994.
55 K. Levenberg, *Q. Appl. Math.*, 1944, **2**, 164.
56 J. J. Moré, in *Numerical Analysis*, ed. G. A. Watson, Springer Berlin Heidelberg, Berlin, Heidelberg, 1978, p. 105.
57 S.-D. Yoh, D.-Y. Cheong, C.-H. Lee, S.-H. Kim, J.-H. Park, M. Fujio and Y. Tsuno, *J. Phys. Org. Chem.*, 2001, **14**, 123.
58 T. B. Phan, C. Nolte, S. Kobayashi, A. R. Ofial and H. Mayr, *J. Am. Chem. Soc.*, 2009, **131**, 11392.
59 S. S. Mirvish, B. Gold, M. Eagen and S. Arnold, *Zeitschrift für Krebsforsch. und Klin. Onkol.*, 1974, **82**, 259.
60 M. J. Crookes and D. L. H. Williams, *J. Chem. Soc., Perkin Trans. 2*, 1989, **9**, 1319.
61 T. Sperger, I. A. Sanhueza and F. Schoenebeck, *Acc. Chem. Res.*, 2016, **49**, 1311.
62 S. Moon, S. Chatterjee, P. H. Seeberger and K. G. Gilmore, *Chem. Sci.*, 2021, **12**, 2931.
63 P. H.-Y. Cheong, C. Y. Legault, J. M. Um, N. Çelebi-Ölçüm and K. N. Houk, *Chem. Rev.*, 2011, **111**, 5042.
64 E. C. Sherer, J. R. Cheeseman and R. T. Williamson, *Org. Biomol. Chem.*, 2015, **13**, 4169.
65 L. Simón and J. M. Goodman, *Org. Biomol. Chem.*, 2011, **9**, 689.
66 K. N. Houk and F. Liu, *Acc. Chem. Res.*, 2017, **50**, 539.
67 O. Engkvist, P.-O. Norrby, N. Selmi, Y. Lam, Z. Peng, E. C. Sherer, W. Amberg, T. Erhard and A. L. Smyth, *Drug Discovery Today*, 2018, **23**, 1203.